Cell shape impacts on the positioning of the mitotic spindle with respect to the substratum

Francisco Lázaro-Diéguez[a], Iaroslav Ispolatov[b], and Anne Müsch[a]
[a]Department of Developmental and Molecular Biology, Albert Einstein College of Medicine, New York, NY 10461;
[b]Departamento de Física, Universidad de Santiago de Chile, 9170124 Santiago, Chile

ABSTRACT **All known mechanisms of mitotic spindle orientation rely on astral microtubules. We report that even in the absence of astral microtubules, metaphase spindles in MDCK and HeLa cells are not randomly positioned along their *x*-*z* dimension, but preferentially adopt shallow β angles between spindle pole axis and substratum. The nonrandom spindle positioning is due to constraints imposed by the cell cortex in flat cells that drive spindles that are longer and/or wider than the cell's height into a tilted, quasidiagonal *x*-*z* position. In rounder cells, which are taller, fewer cortical constraints make the *x*-*z* spindle position more random. Reestablishment of astral microtubule–mediated forces align the spindle poles with cortical cues parallel to the substratum in all cells. However, in flat cells, they frequently cause spindle deformations. Similar deformations are apparent when confined spindles rotate from tilted to parallel positions while MDCK cells progress from prometaphase to metaphase. The spindle disruptions cause the engagement of the spindle assembly checkpoint. We propose that cell rounding serves to maintain spindle integrity during its positioning.**

Monitoring Editor
Wallace Marshall
University of California,
San Francisco

Received: Aug 29, 2014
Revised: Dec 30, 2014
Accepted: Jan 28, 2015

INTRODUCTION

During eukaryotic cell divisions, the bipolar mitotic spindle serves to accurately partition the duplicated chromosome set into each of the daughter cells and thereby ensures genomic stability, one of the most essential aspects of life (Walczak and Heald, 2008). In addition, spindle placement and orientation within the mitotic cell define the position of the cleavage furrow and hence determine the relative cell sizes of the daughters, the symmetric or asymmetric segregation of cell surface domains and organelles, and the placement of daughters within a tissue (Bergstralh and St Johnston, 2014). The spindle parts that have chromosome-separating function are believed to operate independently from those that mediate spindle positioning. In fact, significant knowledge has been acquired from spindle assembly assays in cell-free extracts (Desai *et al.*, 1999). A simplified description of the self-organizing core spindle apparatus in metaphase is that two microtubule (MT)-focusing centrosomes are kept at a defined distance by repulsive forces exerted on the poles by antiparallel, overlapping MTs, which slide against each other, and by the tension of K-fibers, the MT bundles that attach in an amphitelic way to kinetochores of connected sister chromatids and to either centrosome (Dumont and Mitchison, 2009b; Mogilner and Craig, 2010). The result is an ovoid in which the chromosomes are aligned perpendicular to the spindle pole axis equidistantly from both poles. Spindle dimensions are described by the pole-to-pole distance (*s*) and the diameter of the metaphase plate (*p*). The forces that keep the spindle in balance are generated by MT polymerization and depolymerization, MT motors, and the viscoelastic response of the spindle (Dumont and Mitchison, 2009b).

Spindle orientation, on the other hand, is mediated by astral MTs that radially emanate from each centrosome and, in most somatic cells, reach the cell cortex. In cells in which spindle orientation is critically important, astral MTs position the spindle using cortical spatial cues: the MT minus end–directed motor dynein is anchored at discrete cortical regions via protein complexes such as the evolutionarily conserved Gαi/leucine-glycine-asparagine repeat protein (LGN)/nuclear and mitotic apparatus protein (NuMA) module, from where it exerts pulling forces on astral MTs to align the spindle along the line connecting the dynein patches that are located at the opposite domains of the cell (Kotak and Gonczy, 2013; McNally, 2013).

This article was published online ahead of print in MBoC in Press (http://www.molbiolcell.org/cgi/doi/10.1091/mbc.E14-08-1330) on February 5, 2015.
Address correspondence to: Anne Müsch (anne.muesch@einstein.yu.edu).
Abbreviations used: MA, metaphase plate axis; MT, microtubule; SA, spindle pole axis.

In symmetrically dividing cells, the two cortical Gαi/LGN/NuMA patches are placed at equal distance from a cell's basal surface, which results in a parallel orientation of the spindle pole axis to the basal domain and ensures that division occurs within in the plane of the monolayer. Along the cell's *x-y* dimension, tensile forces in actin-based retraction fibers guide the planar orientation of the mitotic spindle by yet incompletely understood mechanisms (Fink *et al.*, 2011; Thery and Bornens, 2006; Thery *et al.*, 2005, 2007). By culturing cells on patterned substrates, it was shown that the placement of retraction fibers is largely defined by the cell's planar shape in interphase (Thery *et al.*, 2005, 2007). In addition, dynamic clusters of filamentous actin (F-actin) in the vicinity of the cell cortex have been suggested to bias astral MT–based cortical attachment (Mitsushima *et al.*, 2010; Fink *et al.*, 2011). Independently of these discrete cortical cues, astral MTs can stably equilibrate the spindle in the geometric cell center by shape-sensing mechanisms that involve pulling or pushing forces that scale with astral MT length (O'Connell and Wang, 2000; Grill and Hyman, 2005; Minc *et al.*, 2011). Such shape-sensing mechanisms can also explain Hertwig's rule, according to which cells with simple elongated shapes along the *x-y* dimension align their mitotic spindle with their long cell axis (Minc *et al.*, 2011). Whereas the role of cell shape has been well explored for the planar orientation of the metaphase spindle (i.e., its orientation within the cell's *x-y* plane), less is known about the contribution of cell shape to spindle positioning along the *x-z* dimension. Failure to establish discrete dynein patches at opposite domains of the lateral cortex such as upon depletion or inhibition of Gαi, LGN, or NuMA (Woodard *et al.*, 2010; Zheng *et al.*, 2010; Peyre *et al.*, 2011; Kotak *et al.*, 2012) upon disruption of cortical actin filaments (Busson *et al.*, 1998) or by inhibiting phosphoinositide 3-kinase–regulated pathways downstream of integrin signaling (Toyoshima *et al.*, 2007; Toyoshima and Nishida, 2007) leads to loss of the stereotypic alignment of the metaphase spindle with the substratum or basal surface and increases the incidence of "tilted" spindles. Whether spindle orientation along the *x-z* dimension is random under these conditions or shape-dependent positioning mechanisms operate in the absence of cortical cues, however, has not been determined. Here we investigated this question, which is important for the outcome of cell divisions in monolayered cells. We determined that in the absence of astral MTs, which participate in all known spindle-positioning mechanisms, metaphase spindle orientation in cultured Madin–Darby canine kidney (MDCK) and HeLa cells became random along the *x-y* plane but remained biased toward a shallow spindle tilt along the *x-z* dimension. We identified the mismatch of spindle and cell dimensions in a population of metaphase cells that exhibited incomplete cell rounding as reason for this bias. We then determined how this spindle confinement affects spindle alignment with the substratum during prometaphase-to-metaphase progression when spindle rotation forces operate under control conditions.

RESULTS

Loss of cortical cues by LGN-knockdown and dynein inhibition does not result in random spindle orientation in MDCK cells

We analyzed metaphase spindle orientation in recently confluent MDCK monolayers by positioning cells such that their spindle pole axis (SA) aligned with the *x-z* plane during confocal sectioning and measured the angle β between SA and the substratum along the *x-z* dimension (Figure 1A and Supplemental Movie S1 for the definition of the parameters). To avoid artifacts in the analysis of the spindle

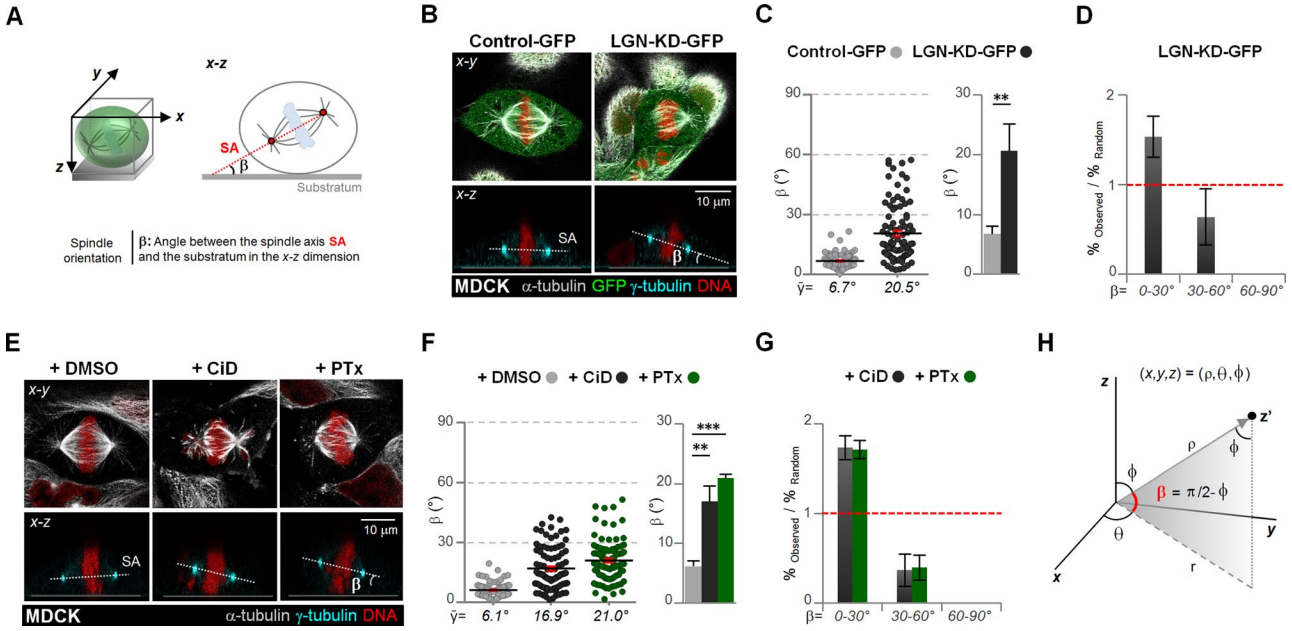

FIGURE 1: Nonrandom *x-z* spindle orientation upon disruption of cortical cues. (A) Definition of mitotic spindle orientation relative to the substratum (β angle). Confocal *x-y* and *x-z* sections of control GFP– and LGN-KD-GFP–expressing MDCK clones (B) or control DMSO-, CiD-, and PTx-treated MDCK cells (E) immunostained as indicated. DNA was stained with DAPI. (C, F) Distribution (left; mean $\bar{y} \pm$ SEM, with dots indicating individual data points) and quantification (right; mean ± SD) of the β angle. The β angle distribution was analyzed for randomness (D, G). The red dashed line marks the $\%_{Observed}/\%_{Random}$ index of 1 expected for each column if the β distribution were random. (B–G) Thirty cells/experiment were analyzed for three independent experiments. (C, F) $^{**}p \leq 0.01$, $^{***}p \leq 0.001$, analyzed by *t* test. (H) Spherical coordinate system on which the randomness calculation is based (see *Materials and Methods* for details).

angle, which can be caused by mounting cells between two glass covers and thus squeezing them flatter, we analyzed mitotic profiles in monolayers on MatTek dishes either in paraformaldehyde (PFA)-fixed cells that were kept in phosphate-buffered saline (PBS) buffer after immunostaining or directly by live-cell imaging.

First, we compared a control cell line stably transduced with a green fluorescent protein (GFP)–encoding lentivirus (control-GFP) to an MDCK cell line stably expressing GFP alongside an LGN-shRNAmir (LGN-knockdown [KD]–GFP), which efficiently suppressed LGN expression (Zheng *et al.*, 2010). Both cell lines had previously been characterized and compared for spindle orientation in three-dimensional MDCK cultures (Zheng *et al.*, 2010). In agreement with this earlier study, which measured spindle alignment with respect to the cell apex, we observed a disruption of mitotic spindle alignment with the basal surfaces in LGN-depleted cells compared with controls (20.5 ± 1.5° vs. 6.7 ± 0.4°, respectively, for the average β angle; Figure 1, B and C). To determine whether this distribution of β angles in LGN-KD cells constitutes a random spindle orientation, we considered the spindle pole axis in a spherical coordinate system (Figure 1H). In this system, our angle β is complementary to the traditional polar angle ϕ, $\beta = \pi/2 - \phi$. In spherical coordinates, the element of the surface area is proportional to $\sin \phi = \cos \beta$. Therefore, for completely random spindle orientation, the frequency of any observed β angle divided by cos β must be a constant. For the analysis, we grouped cells into three bins that are frequently used to describe spindle orientation along the *x*-*z* dimension, 0–30° (parallel to shallow spindle orientation), 30–60° (oblique spindle angles), and 60–90° (near-vertical to vertical spindle orientation; Juschke *et al.*, 2014), and used as an index $\%_{Observed}/\%_{Random}$, which corresponds to the percentage of cells with β angles in each of the three bins divided by the integral of the cosine between the margins of the bins (see *Materials and Methods*). For perfectly random spindle orientation, an index of 1 is expected, which is shown by the red dashed line in Figure 1D. To accept the hypothesis of random orientation, the fraction of cells in each bin should be within 1 SD of that theoretical value. For LGN-KD cells in Figure 1D, however, each bar graph is at least 1 SD above or below the line denoting random spindle angles. LGN-KD cells thus exhibit a nonrandom spindle orientation that is biased toward spindles with a shallow spindle tilt.

We obtained similar results when we pharmacologically inhibited the activity of dynein in metaphase cells with ciliobrevin D (CiD) or blocked the membrane recruitment of Gαi, which in turn recruits LGN, with pertussis toxin (PTx). With both drugs, metaphase spindles lost their parallel spindle alignment with the substratum (Figure 1, E and F), and yet our randomness analysis rejected a random spindle distribution in each case (Figure 1G).

Thus loss of the cortical cues that mediate spindle alignment with the substratum in MDCK cells does not lead to random spindle orientation along a cell's *x*-*z* dimension but biases spindle orientation toward a shallow spindle tilt.

Spindle orientation in MDCK and HeLa cells is nonrandom even when actin polymerization or astral MTs are abolished

We considered two principal mechanisms for the nonrandom spindle positioning in the absence of the cortical Gαi/LGN/dynein cues: 1) F-actin–based structures, such as recently identified clusters of subcortical F-actin that can bias astral MT growth and/or their cortical attachment, and 2) astral MT–dependent cell shape–sensing mechanisms.

In agreement with the original study that described the subcortical actin clusters in HeLa cells but did not detect them in MDCK cells, we also did not observe an obvious "actin cloud" in MDCK cells (Mitsushima *et al.*, 2010; unpublished data), yet we cannot rule out that less conspicuous F-actin structures affect astral MT growth and/or attachment to the cortex. Therefore we analyzed MDCK metaphase spindle positioning after a 1-h latrunculin B (LtB) treatment, which depolymerizes microfilaments (Figure 2A). Of note, LtB was also effective in disrupting the "F-actin cloud" in HeLa cells (Mitsushima *et al.*, 2010). Removal of cortical microfilaments prevents dynein and LGN/NuMA recruitment to the metaphase cortex (Lazaro-Dieguez *et al.*, 2013; unpublished data), which accounts for an increase in the mean β angle from 4.9 ± 0.4° to 33.5 ± 1.9° in fixed cells (Figure 2, A and B) and from 9.4 ± 0.8° to 31.8 ± 2.0° in the live-cell analysis (Figure 2, D and E). Yet, as with LGN and dynein inhibition, spindle orientation in LtB-treated MDCK cells was nonrandom (Figure 2, C and F), making it unlikely that actin filament–based mechanisms account for nonrandom spindle orientation in the absence of the LGN/NuMA/dynein cues.

To assess metaphase spindle orientation in the absence of astral MTs, we used nocodazole (NZ), a drug that interferes with MT polymerization. At low doses, NZ selectively depolymerizes astral spindle MTs and also reduces the number of polar MTs, which exhibit high turnover, but it leaves intact the metaphase K-fibers that are capped by kinetochores at their plus ends and anchored by centrosomes at their minus ends (O'Connell and Wang, 2000; Maiato *et al.*, 2004; Emanuele and Stukenberg, 2007; Toyoshima and Nishida, 2007; Figure 2A; +NZ). NZ treatment increased the mean β angle from 4.9 ± 0.4° to 27.6 ± 2.1° in fixed cells (Figure 2B) and from 9.4 ± 0.8° to 26.9 ± 2.0° in the live-cell analysis (Figure 2E). However, even without astral MTs, metaphase spindle orientation was biased toward shallow β angles. We made similar observations in HeLa cells (Supplemental Figure S1, A–C). These findings were indeed unexpected because astral MTs mediate all known spindle alignment mechanisms.

Nonrandom distribution of β angles in the absence of astral MTs is due to incomplete cell rounding

What, then, is the reason for the overrepresentation of spindles with shallow β angles in the absence of astral MT–sensing mechanisms? We noticed that in many of the MDCK NZ-metaphase profiles with shallow β angle the metaphase plate appeared in contact with the cell apex, base, or both, whereas chromatin in cells with steeper β angles was always clear of the cell perimeter in *x*-*z* views and in three-dimensional (3D) views and models (Figure 3 and Supplemental Movie S2). We therefore explored the hypothesis that the spindle dimensions are too large to allow free positioning in all cells and that for a large mitotic spindle, the diagonal fit is the only position possible.

For unconfined spindle rotation the cell's *x*′, *y*′, and *z*′ dimensions must exceed *s* and *p* (see schematic in Figure 4A and Supplemental Movie S1). We determined that of the metaphase cell's mean *x*′, *y*′, and *z*′ dimensions, cell height, *z*′, was the shortest in both control and NZ-treated MDCK cells (Figure 4B), indicating that not all cells are spherical during mitosis. The average ratios of measured *z*′ to *s* and to *p* in NZ-treated cells was 1.49 ± 0.23° and 1.16 ± 0.19°, respectively (Figure 4C). When we divided the cell population into one above and one below the average for *z*′/*s* and *z*′/*p*, respectively, and assessed their β angle distributions separately, it became apparent that whereas the cell population with higher *z*′/*s* and *z*′/*p* featured in fact random spindle orientation, cells with low *z*′/*s* and *z*′/*p* distributed their metaphase spindles nonrandomly (Figure 4D).

The lack of clearance could either be caused by a mismatch of spindle and cell size or result from incomplete cell rounding. In support of the latter, we found chromatin infarctions with the cortex restricted to flatter cells (Figure 3B). Cell roundness in this analysis was described by a circularity index in the *x*-*z* plane, $C_{x\text{-}z}$,

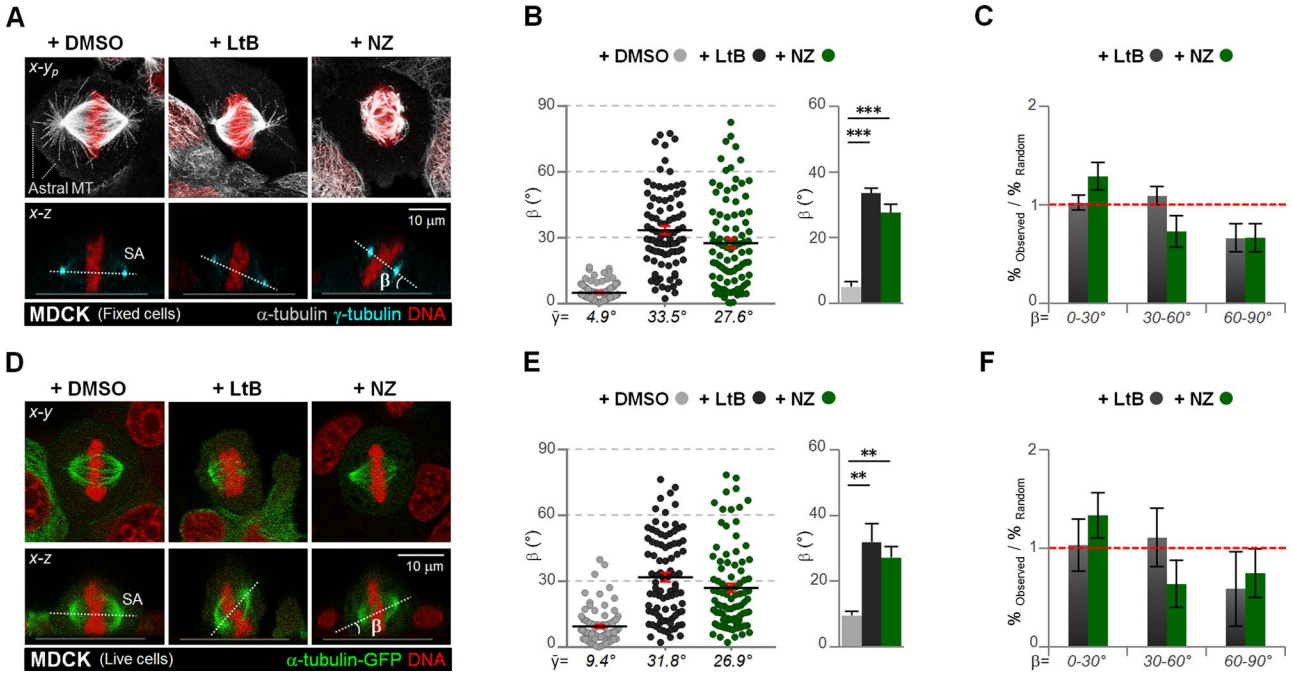

FIGURE 2: The *x-z* spindle orientation is nonrandom when microfilaments or astral microtubules are depolymerized. Confocal *x-y* projections (x-y_p) and *x-y* and *x-z* sections of control DMSO-, LtB-, and NZ-treated MDCK cells were recorded after cell fixation and staining with the indicated antibodies and DAPI (A) or by live imaging in MDCK cells expressing α-tubulin–GFP and stained with DRAQ5 (D). (B, E) Distribution (left; mean $\bar{y} \pm$ SEM, with dots indicating individual data points) and quantification (right; mean ± SD) of the β angle. The β angle distribution was analyzed for randomness (C, F). The red dashed line marks the index expected for each column if the β distribution were random. Error bars indicate mean ± SD. (A–F) Thirty cells/experiment were analyzed for three independent experiments. (B, E) $^{**}p \leq 0.01$, $^{***}p \leq 0.001$, analyzed by *t* test.

where a value of 1 describes completely round cells (see schematic in Figure 4A and Supplemental Movie S1). The $C_{x\text{-}z}$ of NZ-treated cells with β angles in the 60–90° bin was larger than the $C_{x\text{-}z}$ of cells in the 30–60° bin (Figure 4E, right). When we plotted the β angles against $C_{x\text{-}z}$ a larger spreading of β angles was apparent in the rounder than in the flatter cells (Figure 4F, left). To test further how higher circularity $C_{x\text{-}z}$ correlated with a larger spread of β angles in NZ-treated cells, we binned metaphase cells according to their $C_{x\text{-}z}$ index in intervals of 0.05 from 0.55 to 1 and plotted the SDs of their corresponding β angles against the $C_{x\text{-}z}$ bins. A good, statistically significant, positive correlation (r = 0.74, p = 0.02) between both parameters was indeed apparent (Figure 4F, right). Furthermore, when we divided the NZ-treated metaphase cell population into one above and one below the average for $C_{x\text{-}z}$ (Figure 4E, left), we observed random distribution of β angles in cells with higher but not lower $C_{x\text{-}z}$ (Figure 4G). We made similar observations in HeLa cells (Supplemental Figure S1, D and E).

To test directly whether cell flattening causes spindles to orient with smaller β angles upon NZ treatment, we compressed MDCK monolayers with a pressure of 2 kPa (Supplemental Figure S2), which significantly reduced z' and β in NZ-treated cells (Supplemental Figure S2B). We made similar observation when we followed z' and β by live-cell analysis upon compression in NZ-treated cells (Supplemental Figure S2C).

Note that cell shape only affected spindle positioning along the *x-z* dimension. We never observed any contacts between the mitotic apparatus and the cell cortex along the *x-y* dimension in NZ-treated MDCK cells (Figure 3). The angle δ between SA and maximum cell dimension in the *x-y* plane (see schematics in Supplemental Figure S3A) showed no correlation with cell circularity along the *x-y* dimension, $C_{x\text{-}y}$ (Supplemental Figure S3B).

We conclude that randomization of metaphase spindles upon removal of astral MTs is hindered by the geometric constrains presented by the cell's height, whereas there are no such constraints in the *x-y* plane, and the spindle randomizes its orientation along this plane. For rounder cells, which are taller, there are fewer constraints, and the *x-z* spindle position is more random.

Randomization in round cells could occur when metaphase spindles, aligned parallel to the substratum at the time of NZ addition, diffuse to equilibration after loss of their cortical anchors. We estimated from *x, z, t* time-lapse movies taken at 10-s intervals over 4 min in six round, NZ-treated metaphase cells that diffusion would take ~3 h to randomize the spindle (Supplemental Figure S4). However, if prophase and prometaphase spindles, which have a larger spread of β angles (Reinsch and Karsenti, 1994; Supplemental Figure S5, A and B), also contribute to the metaphase population that we score after the 1-h NZ treatment, randomization does not require that spindle diffusion reaches its equilibrium. Our data indicate that the latter indeed applies. In MDCK cells, 30% of all mitotic profiles are cells in prophase and prometaphase, compared with 50% that are in metaphase at steady state (Supplemental Figure S6A), and we determined that these cells progress to metaphase in the presence of NZ (Supplemental Figure S6, B and C). Whereas cells are significantly flatter in prometaphase ($C_{x\text{-}z}$ = 0.63) than in metaphase ($C_{x\text{-}z}$ = 0.86), we observed a near-random spindle distribution in prometaphase cells with above-average circularity (Supplemental Figure S5C). By contrast, the flat population showed a clear bias toward shallow β angles. Thus hindered diffusion after astral MT removal,

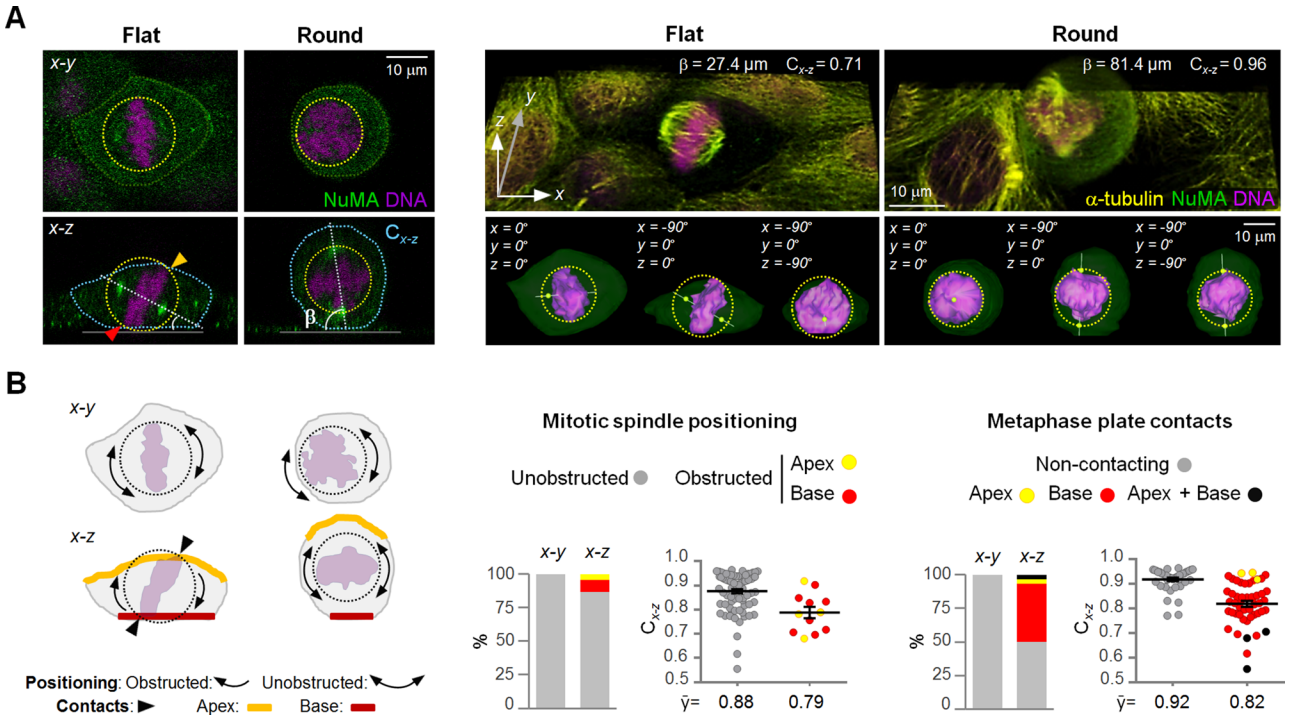

FIGURE 3: Confinement prevents random *x-z* orientation of metaphase spindles upon astral-MT depolymerization in MDCK cells. (A) NZ-treated MDCK cells from Figure 2A were analyzed for confinement of the mitotic spindle. A representative cell with flat or round shape along the *x-z* dimension is shown (left, *x-y* and *x-z* confocal sections; right, 3D views and models, top and bottom, respectively). The yellow dashed circle represents the dimension required for unobstructed positioning of the mitotic spindle. Yellow and red arrowheads indicate contacts of the metaphase plate with the cell apex or base, respectively. (B) Left, schematic of the analysis of metaphase plate positioning in flat and round cells along the *x-y* and *x-z* dimensions. Middle, percentage of cells in which a circle encompassing the mitotic spindle stayed clear of the cell contours (gray) or intersected with the cell apex or base (red and yellow) in *x-y* or *x-z* sections, respectively. Cells were grouped according to unobstructed (gray data points) and obstructed (red and yellow data points) spindles, and the $C_{x\text{-}z}$ values for each group were plotted. Right, percentage of cells in which no contact of the cell cortex with the metaphase plate was apparent (gray) and of cells in which either base or apex (red and yellow) or both (black) touched the chromatin plate. Cells were grouped according to noncontacting (gray data points) and contacting (red/yellow/black data points) chromatin plates, and the $C_{x\text{-}z}$ values for each group were plotted. Of note, obstructed spindles and metaphase plate contacts with the cell cortex were more frequent in cells with lower $C_{x\text{-}z}$. Error bars indicate mean ± SEM. Thirty cells/experiment were analyzed for three independent experiments.

together with a strong bias toward shallow spindle orientation in prometaphase, likely causes the nonrandom spindle orientation that we score in the flat-cell metaphase population after 1 h of NZ treatment.

Cell rounding is required to maintain spindle integrity during its metaphase rotation by astral MT–based cues

A corollary of our findings is that confined metaphase spindles, in the absence of astral MTs, did not acquire random positioning by pushing the cell cortex outward to allow their free rotation. Because low doses of NZ not only abolish astral MTs but also promote rounder cells with shorter spindles compared with controls, control MDCK cells had even smaller average z'/p ratios in metaphase than NZ-treated cells (Figure 4C). We therefore wondered how MDCK cells accomplish their stereotypic spindle orientation in confinement. We considered two principal scenarios: 1) cells assemble their metaphase plate after astral MTs are already anchored to cortical cues, that is, after the spindle position is set, or 2) cells rotate their spindles in place during or after metaphase assembly. In the first scenario, metaphase plate diameter p and cell height z' would evolve as a result of the vertical, outward-directed pushing forces of the spindle and the resistance of the cortex. In the second scenario, the torque applied on the spindle poles by astral MTs would push the cortex outward to allow spindle rotation.

To discriminate between the two scenarios, we monitored the β angle as MDCK cells progressed from prometaphase to metaphase, using *x*, *z*, *y* time-lapse microscopy and analysis of fixed cells. Live-cell analysis of seven prometaphase cells revealed a progressive decrease of their β angles between prometaphase and metaphase (Figure 5A). To evaluate mitotic progression in fixed cells, we assigned the chromatin a circularity (C_c) value: chromatin with many unattached kinetochores in early prometaphase was best described by a round shape, whereas the assembled metaphase disk had the lowest circularity (Figure 5B). We found that decreasing C_c correlated with decreasing β angles in a monotonous manner in MDCK as well as in HeLa cells, suggesting that chromosome and spindle alignment go hand in hand in both cell lines (Figure 5C). Thus our data are consistent with a scenario in which confined spindles undergo rotation.

During our live-cell analysis of the prometaphase-to-metaphase transition, we noticed that flat cells sometimes featured deformed spindles in which the angle ε between the SA and metaphase plate axis (MA) deviated from the 90° that is characteristic of the force-balanced metaphase spindle. This defect was visible early after

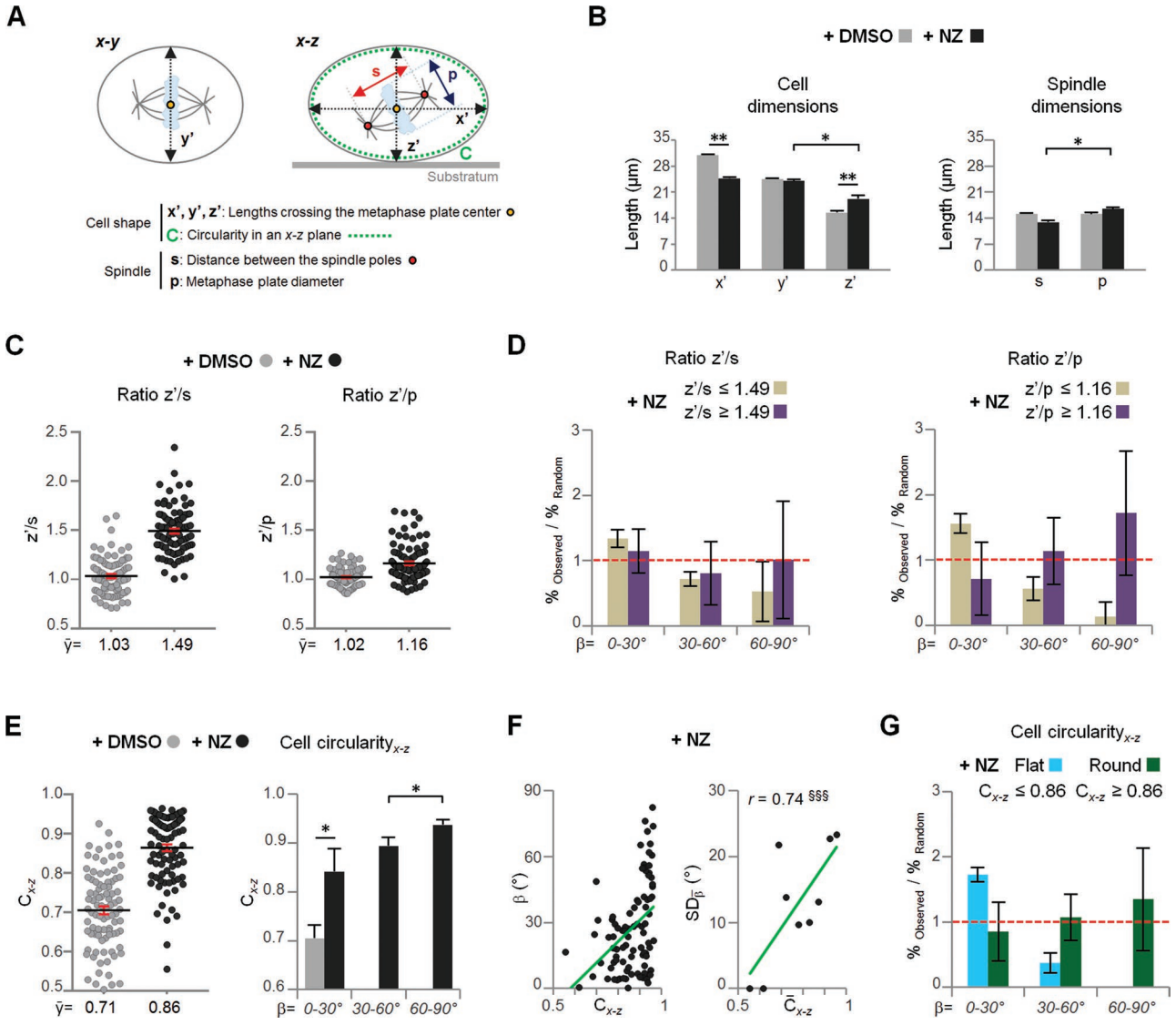

FIGURE 4: Cell rounding randomizes *x-z* metaphase spindle orientation in the absence of astral MTs. (A) Definition of the parameters measured: cell dimensions (x', y', z'), cell circularity in the *x-z* plane ($C_{x\text{-}z}$), distance between spindle poles (s), and metaphase plate diameter (p). (B–G) Cells analyzed in Figure 2A were quantified for x', y', z', s, and p (B) and $C_{x\text{-}z}$ (E). The distribution of the ratios z'/s and z'/p (C) and of $C_{x\text{-}z}$ (E; left) were plotted as individual data points for control and NZ-treated cells (mean $\bar{y} \pm$ SEM, where dots indicate individual data points). $C_{x\text{-}z}$ was quantified (mean ± SD; E; right). (F) Left, relation between the β angle and $C_{x\text{-}z}$ plotted in a scatter diagram. Note the increase in β angle spreading at higher $C_{x\text{-}z}$. Right, when NZ-treated cells were binned according their $C_{x\text{-}z}$ index in intervals of 0.05 from 0.55 to 1, a positive correlation between the SDs of mean β and mean $C_{x\text{-}z}$ for each category was observed that is significant ($^{\S\S\S}p \leq 0.001$). Green lines correspond to the trend line. (D, G) The β angle distribution in NZ-treated cells was interrogated for randomness after cells were grouped by above- and below-average z'/s, z'/p, or $C_{x\text{-}z}$ (flat or round), respectively. The index 1 for randomness is marked with a red dashed line. Error bars indicate mean ± SD. (B–G) Thirty cells/experiment were analyzed for three independent experiments. (B, E) $^{*}p \leq 0.05$, $^{**}p \leq 0.01$, analyzed by *t* test.

spindle alignment with the substratum but gave way to the characteristic perpendicular orientation of the MA to the SA in the assembled metaphase plate at later time points (Figure 6A). In fixed cells, metaphase spindles with ε angles >90° stained positive for BUBR1, a spindle assembly checkpoint protein that is present on unattached chromatids (reviewed in Wang *et al.*, 2014). This observation indicates that the spindle deviation reflected incomplete amphitelic kinetochore–MT attachment and/or lack of tension between sister chromatids (Figure 6B). Indeed, in some cells, breaks in the straight MA were apparent in *x-z* views, indicating that individual K-fibers had relaxed or snapped (Figure 6D, cell 2). Quantitative analysis of fixed cells revealed that the higher ε angles were characteristic of flat cells, that is, the population of cells that had a low z'/p ratio or $C_{x\text{-}z}$ index (Figure 6C). To establish whether the spindle deformation was contingent on spindle alignment forces, we measured the ε angle of cells in the presence of NZ and compared it to ε after NZ washout (Figure 6D). NZ washout allowed the reformation of astral MTs (Supplemental Figure S7A) and caused the alignment of the metaphase SA parallel to the substratum in both round and flat cells, as determined by live-cell imaging in seven round and seven flat cells (Supplemental Figure S7C). Similarly, β angles measured in cells fixed 45 min after NZ washout dropped close to those

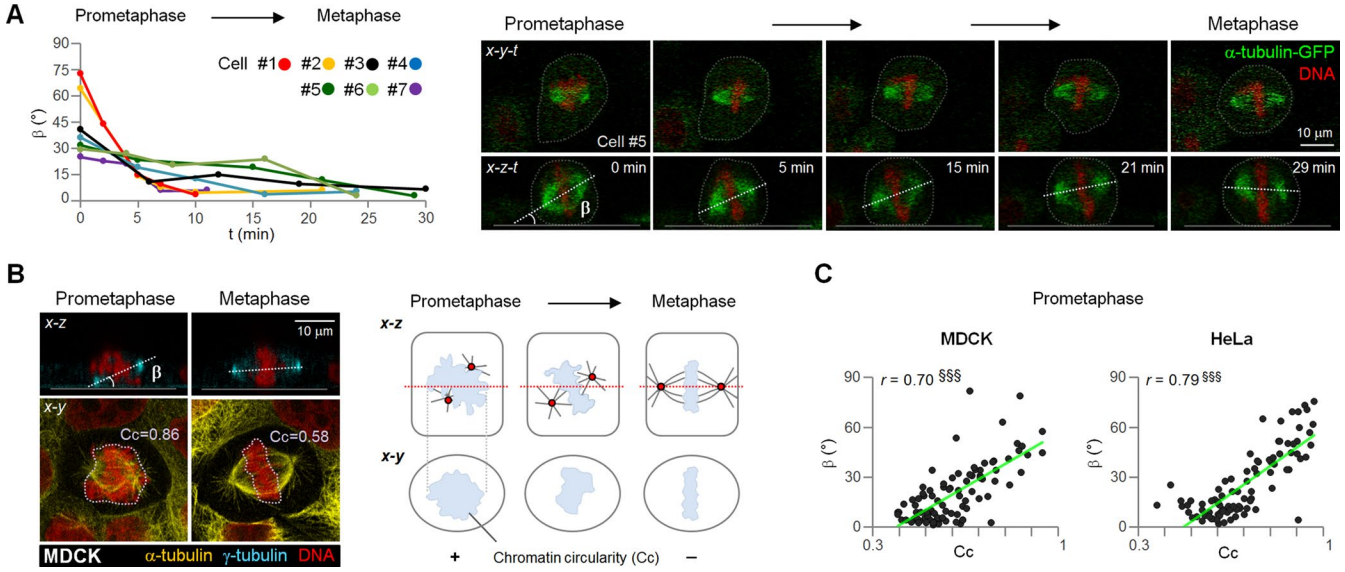

FIGURE 5: Horizontal spindle orientation occurs concomitant with metaphase plate assembly. (A) Left, the β angle was quantified during the transition from prometaphase to metaphase in MDCK cells expressing α-tubulin–GFP and labeled with DRAQ5. Right, sequential *x-y-t*/*x-z-t* confocal time-lapse (cell 5). (B,C) Confluent MDCK and HeLa cell cultures were fixed and immunostained as indicated. DNA was labeled with DAPI. Cells were analyzed for the chromatin circularity (C_c; light blue shapes in schematics) in single confocal *x-y* sections between the two spindle poles (dashed red lines in schematics). (C) Correlation analysis between β and C_c in prometaphase profiles (green trend lines). Thirty cells/experiment were analyzed for three independent experiments. §§§$p \leq 0.001$ for the Pearson coefficient.

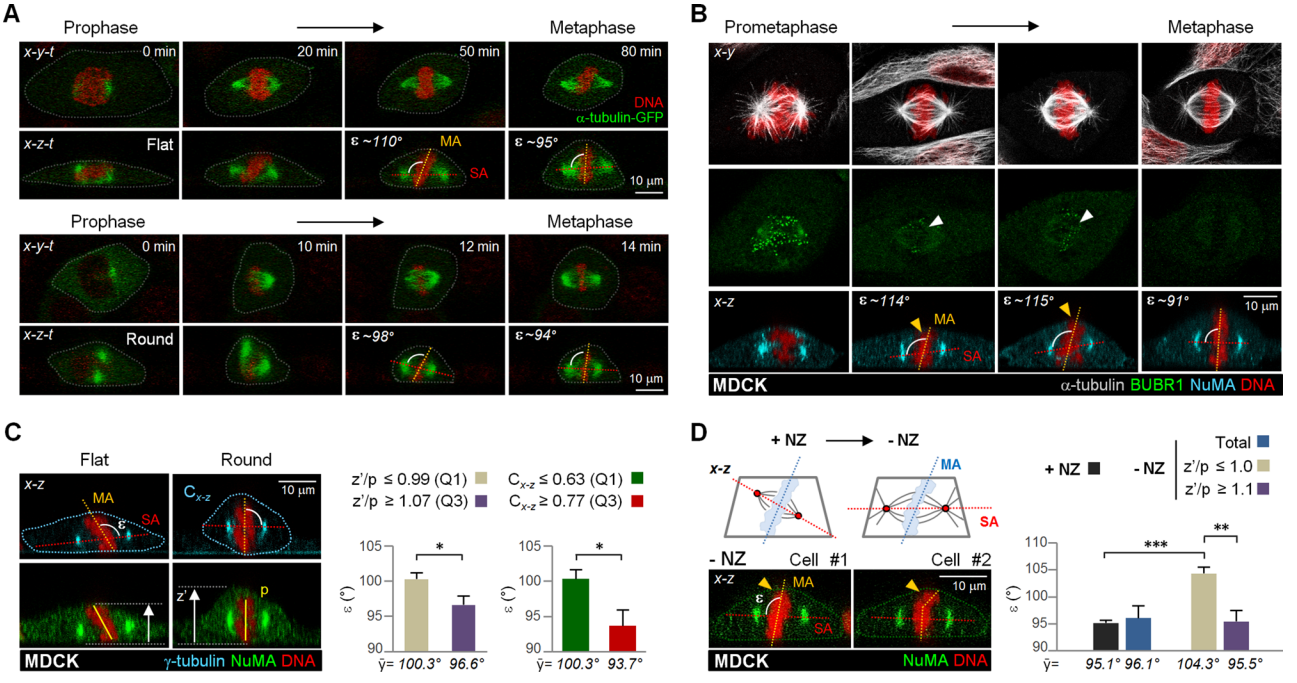

FIGURE 6: Confinement interferes with the perpendicularity between the spindle pole axis and the metaphase plate during astral MT–mediated spindle alignment. (A) Sequential *x-y-t*/*x-z-t* confocal time-lapse series after the transition from prophase to metaphase in DRAQ5-stained MDCK cells expressing α-tubulin–GFP with flat and round shape. Note the increase of the maximum angle ε between the spindle axis (SA) and the metaphase plate axis (MA) in flat cells. (B) BUBR1, a spindle assembly checkpoint protein, was detected in prometaphase profiles and in metaphase profiles (white arrowheads) with high ε. (C) MDCK cells fixed and stained as indicated were grouped by their lower and upper *z'/p* ratios and $C_{x\text{-}z}$ (below and above quartiles Q1 and Q3, respectively) and their ε angle was determined. Thirty cells/experiment were analyzed for three independent experiments. (D) The ε angle was measured in cells from Supplemental Figure S7A. The NZ-washout population was grouped by its upper and lower *z'/p* ratios. (B, D) Yellow arrowheads indicate contacts between the cell apex and the metaphase plate. (C, D) Error bars indicate mean ± SD. *$p \leq 0.05$, **$p \leq 0.01$, ***$p \leq 0.001$, analyzed by *t* test.

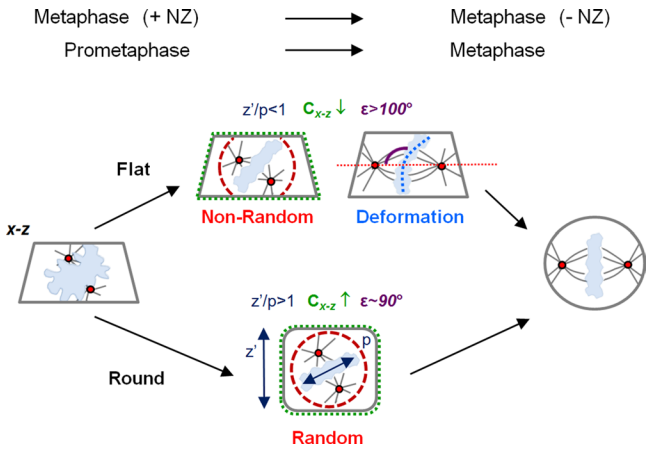

FIGURE 7: Summary and model. When mitotic cells are subjected to low doses of NZ, which depolymerizes their astral MTs, the resulting metaphase spindle orientation along a cell's *x-z* dimension is governed by cell shape. In round cells with high *z′/p* ratio and C_{x-z}, the mitotic spindle adopts a random *x-z* orientation. This randomization is the result of unconstrained spindle diffusion from the original positions, which are substrate parallel in the case of metaphase spindles and random in the prophase and prometaphase spindles that progress to metaphase in the absence of astral MTs. When confined by the cell cortex in flat cells, by contrast, spindles are biased toward shallow spindle tilts because their diffusion is hindered and their prometaphase orientation is already biased by shape. NZ washout aligns metaphase spindles with the substratum in round and flat cells, but confinement in flat cells frequently leads to spindle deformation during its rotation, such that the metaphase plate deviates from its perpendicular orientation to the spindle pole axis ($\varepsilon \neq 90°$). This rotation-dependent spindle disruption also occurs during prometaphase-to-metaphase progression in unmanipulated control cells that fail to round up sufficiently. The deformed spindles engage the spindle assembly checkpoint and need to be properly reassembled before anaphase progression.

measured in control cells (Supplemental Figure S7B). Of note, within this time period after NZ washout, most metaphase profiles from before the washout were maintained, and we did not observe new metaphases forming (unpublished data). Thus NZ washout caused metaphase spindle rotations that led to spindle pole alignment with the substratum. In some of the newly rotated spindles, however, ε significantly deviated from 90°, which was never observed in metaphase spindles before NZ-washout (Figure 6D, +NZ).

Our analysis thus revealed that the cortical forces that operate on astral MTs to rotate the spindle can disrupt the force balance within the core metaphase spindle in situations in which the metaphase plate does not clear the cortex. Such spindle disruptions then require the reassembly of the metaphase spindle after its horizontal alignment, which would delay mitotic progression.

DISCUSSION

The metaphase spindle scales with cell size, as exemplified by the extreme case of reductive cell division in early *Xenopus* embryogenesis (Wuhr *et al.*, 2008; Hazel *et al.*, 2013), and the spindle pole axis is maintained at a reasonably constant length in a given cell type (Goshima and Scholey, 2010). Mitotic cell height and metaphase plate diameter also appear coordinated: spindle size correlates with the amount of chromatin (Dinarina *et al.*, 2009), and immortalized cells with few chromosomes, and hence a short metaphase plate, tend to remain flatter during mitosis than do cells with a higher chromosome number, which assemble longer metaphase plates (discussed in Lancaster *et al.*, 2013). Does this coordination guarantee that spindles can rotate without encountering resistance from the cell cortex while aligning with spatial cues? Our findings in MDCK and HeLa cell cultures reveal that cell and spindle dimensions are in fact not adapted to each other sufficiently to prevent constraint of the metaphase core spindle by the cell cortex in a substantial fraction of mitotic cells (Figure 7). We conclude this from experiments in which the removal of active spindle alignment mechanisms did not yield random spindle orientation along the cell's *x-z* dimension. That the bias toward an orientation with an angle of ~20–30° to the substratum was imposed by cell height and not due to insufficient equilibration into a random position was deduced from 1) the observation that when metaphase cells were divided into populations with below- and above-average ratios of cell height to spindle pole axis or metaphase plate diameter, only the population with the lower ratios showed a spindle-positioning bias toward shallow tilt angles; 2) 3D reconstructions that showed the metaphase plate touching the cell cortex in flat cells with shallow-tilted spindles but not in tall cells featuring vertically oriented spindles; and 3) the fact that compression of the cell monolayer increased the incidence of shallow-tilted metaphase spindles.

The observed spindle infarctions with the cortex are likely the result of insufficient mitotic cell rounding rather than a mismatch between cell volume and spindle size. We infer this from the strong positive correlation between cell circularity in *x-z* planes and larger spindle angle spread and from the fact that we only observed the spindle touch the cortex along the cell's height *z′*, which is the shortest of the cell's dimensions. Spindle orientation with respect to the long cell axis along the *x-y* dimension was in fact random upon NZ treatment.

Although it is established that MDCK spindles exhibit stereotypic substrate-parallel orientation first in metaphase (Reinsch and Karsenti, 1994), the process leading to that orientation had not been characterized. We report here that metaphase spindle alignment is a gradual process that goes hand in hand with chromosome capture as cells progress from prometaphase to metaphase. We determined that spindles rotate from positions with larger β angles to smaller β angles in this process and that rotation occurs even in confinement, that is, when the spindle does not clear the cortex. The latter observation is evidence that astral MT-based rotation forces overcome the resistance of the cortex that prevents spindles in the absence of astral MTs from freely rotating. However, the rigidity of the cortex prevented the metaphase plate from maintaining its perpendicular orientation to the spindle pole axis in the population of cells with *z′/p* ratio <1. In cells with low *z′/p* ratios, the tug of interactions, that is, 1) the torque applied by the astral MTs, 2) the spindle compression forces exerted by the cortex, and 3) the viscoelastic response of the spindle, can result in spindle deformation. It is conceivable that K-fibers either lost tension or decompressed in one half of the spindle relative to the other. The deformed spindles likely require proper amphitelic reestablishment of kinetochore–MT attachments to pass the spindle attachment checkpoint for progression through anaphase. Indeed, live-cell imaging showed that spindle deformations observed early after horizontal spindle pole alignment appeared to be corrected at later metaphase time points. The adaptation likely involves spindle widening and lengthening of its pole-to-pole distance, as observed upon experimental flattening of metaphase cells with already horizontally aligned spindles (Dumont and Mitchison, 2009a). A correlation between cell width and spindle length has indeed been observed in MDCK cells (den Elzen *et al.*, 2009).

The importance of mitotic cell rounding for proper spindle morphogenesis has recently been appreciated (Cadart *et al.*, 2014) based on a study that showed chromosome capture defects and spindle pole splitting in HeLa cells that were experimentally manipulated to assume an extremely flat mitotic cell shape. When cell height was <8 µm, spindle MT length became limiting for efficient MT–kinetochore capture and for assembly of a longer bipolar spindle (Lancaster *et al.*, 2013). Here we provide an additional reason for cell rounding: to maintain spindle integrity during its positioning. The rotation-induced spindle deformations that we attribute to confinement are far more sensitive to cell shape than those reported by Lancaster *et al.* (2013), as they occurred in unmanipulated epithelial cell cultures. Although unlikely to disrupt mitosis, repair of deformed spindles is expected to cause a delay in mitotic progression.

The absence of cortical spindle positioning cues is commonly associated with aberrant cell divisions and loss of monolayer organization in epithelial cells. Our findings make it clear that this cannot be automatically presumed but depends on cell shape and the extent of mitotic cell rounding. Although the highly columnar shape of *Drosophila* wing disk epithelial cells dictates a vertical spindle orientation in the absence of cortical cues that resulted in divisions out of the monolayer exclusively (Nakajima *et al.*, 2013), the more cuboidal shape of MDCK cells, combined with their inefficient mitotic rounding (den Elzen *et al.*, 2009; Mitsushima *et al.*, 2010; and this study), makes such aberrant divisions much less frequent in these cells. This is particularly apparent in 3D cultures that are used to study the relationship between aberrant spindle orientation and tissue organization. The hollow cysts with a single lumen that form under control conditions in 3D MDCK or intestinal cell line cultures are contingent on symmetric divisions in which cells stay within the monolayer, whereas frequent divisions out of the monolayer are expected to result in a solid cell mass. In the absence of spindle alignment mechanisms, cysts generally maintained multiple large lumina, indicating that divisions out of the monolayer were indeed infrequent (Jaffe *et al.*, 2008; Qin *et al.*, 2010; Zheng *et al.*, 2010).

Note that although the nonrandom β angle distribution after disruption of the cortical alignment cues in LGN-KD cells or upon PTx, CiD, or LtB treatment resembled that after NZ treatment, spindle positioning in the former cases could result not only from cortical constraint, but also from MT-dependent shape-sensing mechanisms. Astral MT–based forces that scale with MT length are expected to guide spindles toward smaller β angles in flat cells and are consistent with a larger β angle spread in round cells (Minc *et al.*, 2011), similar to what we described for spindle orientation the absence of astral MTs. "Active" and "passive" cell shape–dependent spindle positioning therefore likely work in congruence.

In summary, although cells do not rely on shape when defining their division axis along the *x-z* dimension as they do for the planar orientation of the division axis, mitotic cell height becomes decisive when lateral cues fail.

MATERIALS AND METHODS

Cell lines and culture

MDCK cells (provided by K. Mostov, University of California at San Francisco, San Francisco, CA) and HeLa cells (CCL-2; American Type Culture Collection, Manassas, VA) were grown in DMEM without phenol red (17-205-CV; Corning, Pittsburgh, PA) supplemented with 10% fetal bovine serum (S11050; Atlanta Biologicals, Flowery Branch, GA) and 2 mM L-glutamine. Stable MDCK cells lines expressing α-tubulin–GFP were generated from parental MDCK cells (Clontech (Clontech, Mountain View, CA). Control GFP– and LGN-KD-GFP–expressing MDCK clones were provided by Q. Du (Medical College of Georgia, Augusta, GA). Cells were maintained at 37°C in a 5% CO_2 humidified atmosphere. For experiments, MDCK or HeLa cells were plated on water-prewashed MatTek dishes or four-compartment CELLview chambers (627870; Greiner Bio-One, Monroe, NC) for live-imaging simultaneous multiplex analysis at 1.5×10^5 cells/cm^2. CiD and PTx were used at 50 µM and 0.5 µg/ml for 60 min or 3 h, respectively. Microfilaments or astral MTs were selectively depolymerized by treating cells with LtB (2 µM) or low doses of NZ (100 nM) for 60 min, respectively. Dimethyl sulfoxide (DMSO) treatment (<0.1% vol/vol) was used as control.

Antibodies and reagents

The following antibodies were used in this study: α-tubulin (ab6160; Abcam, Cambridge, MA), γ-tubulin (T6557; Sigma, St. Louis, MO), BUBR1 (200-301-902; Rockland, Limerick, PA), and NuMA (ab36999; Abcam). Ciliobrevin D, pertussis toxin, and nocodazole were from EMD Millipore (Billerica, MA). Latrunculin B and 4,6-diamidino-2-phenylindole (DAPI) and phalloidin–tetramethylrhodamine isothiocyanate were from Sigma. DRAQ5 was from Invitrogen (Carlsbad, CA).

Immunofluorescence and confocal microscopy

For immunofluorescence experiments, cells were fixed in 4% PFA in PBS buffer for 20 min at room temperature. Cells were permeabilized in 0.1% saponin-1% bovine serum albumin for 20 min before antibody incubation. F(ab')$_2$ fragment secondary antibodies coupled to DyLight 488, Rhodamine Red-X, or DyLight 649 were used. Chromatin was stained with DAPI or DRAQ5 in fixed or time-lapse experiments, respectively. Microscopy was performed in a TCS SP5 confocal microscope (Leica Microsystems, Heidelberg, Germany) equipped with a motorized *x-y-z* stage for multiple position finding and with an 8000-Hz resonant scanner. Cells were imaged using a HCX PL APO 40×/1.25–0.75 oil CS objective on MatTek or CELLview chambers. Confocal (pinhole, 1 Airy unit [AU]; pixel size, 151.7 nm) *x-y-z* stacks or *x-z* sections were taken from the monolayer. The *x-y-z* stack projections (*x-y*$_p$) are shown in some figures as indicated. Live-cell imaging was performed on MatTek or CELLview chambers at 37°C in a CO_2-enriched atmosphere in growth medium without phenol red. The *x-y-z-t* or *x-z-t* stacks (pinhole, 3–4 AU; pixel size, 189.6–379.2 nm) were recorded. Image stacks were processed with LAS AF, version 2.6.0.7266 (Leica Microsystems CMS, Wetzlar, Germany), and ImageJ, version 1.47 (National Institutes of Health, Bethesda, MD). For 3D modeling, *x-y-z* stacks (1 µm/section) were processed in IMOD, version 4.5.7 (http://bio3d.colorado.edu/imod/).

Randomness analysis and calculation of diffusion coefficient

For randomness analysis, we define our spherical coordinate system as having the *x-y* plane parallel to the substratum and the *x-z* dimension describing the cell height *z*′ over the substratum. The *x*-axis is aligned with the projection of the spindle onto the *x-y* plane. In this coordinate system, the spindle always lies in the *x-z* plane. In the corresponding spherical coordinate system, the orientation of the spindle pole axis relative to the *x-y* plane is characterized by elevation ("latitude") angle β, which is complementary to the traditional polar angle ϕ, $\beta = \pi/2 - \phi$. In spherical coordinates, the element of the surface area is proportional to $\sin \phi = \cos \beta$. Therefore, for the completely random spindle orientation, the frequency of any observed β angle divided by cos β must be a constant. For the analysis, we used an index that corresponds to the percentage of cells with β angles in one of the three bins (0–30, 30–60, 60–90°) divided by the integral of the cosine between the margins of the bins, that is, sin 30 − sin 0 = 0.5 for the first bin; sin 60 − sin 30 = 0.366 for the

second bin, and sin 90 − sin 60 = 0.134 for the third bin. In the ideal case of completely random orientation of the spindle, $N = 1$ in each bin. In our analysis, we considered the orientation random when the index ($\%_{Observed}/\%_{Random}$) for each bin was within 1 SD of 1.

To determine the diffusion coefficient, *D*, we analyzed six round, NZ-treated metaphase cells by *x*-*z*-*t* time-lapse imaging in 10-s intervals for 4 min and recorded the deviation of the β angle from its original position from each frame. We plotted $(\beta_{time} - \beta_{time\ =\ 0})^2$ versus time. We determined *D* from the slope of the regression line for the best linear fit of the data that pass through the point $y = 0$, $t = 0$. The time for complete diffusional randomization of spindle orientation is estimated as $[(90°)]^2/D$.

Quantification and statistical analysis

The circularity index *C* (= 4π(area/perimeter^2)) was used to quantify the roundness of a two-dimensional object corresponding to the cross section of the cell by a plane. The measurements of the circularity ($C_{x\text{-}y}$, $C_{x\text{-}z}$, and C_c), the cell and spindle dimensions *x*′, *y*′, and *z*′ and *s* and *p*, respectively, and the β, δ, and ε angles were obtained with ImageJ tools in *x*-*y* and *x*-*z* confocal sections. For measurements of circularity, we drew regions of interest in the perimeter of the cell ($C_{x\text{-}y}$, $C_{x\text{-}z}$; see Supplemental Movie S1) or chromatin (C_c). The location of the spindle poles for β, δ, and ε measurements was determined with α-tubulin–GFP (live cells) and γ-tubulin or NuMA (fixed cells). We ensured that both spindle poles were contained in the *x*-*z* confocal plane sections. For statistical computation and estimation of significance, we used Prism, version 6.0 (GraphPad, La Jolla, CA). Statistical significance was determined using two-tailed unpaired *t* test for three independent experiments. Pearson's coefficient was applied for correlation analysis.

ACKNOWLEDGMENTS

We are grateful to Quansheng Du for the LGN-KD/GFP and GFP-control MDCK clones and Dawn Fernandez for validating the LGN-knockdown efficiency by semi-quantitative PCR. We thank the Müsch lab for critical discussions throughout the course of the study and the anonymous reviewers for input on the manuscript. This work was supported by National Institutes of Health Grants RO1 DK064842 and CA160790 to A.M.

REFERENCES

Bergstralh DT, St Johnston D (2014). Spindle orientation: what if it goes wrong? Semin Cell Dev Biol 34, 140–145.

Busson S, Dujardin D, Moreau A, Dompierre J, De Mey JR (1998). Dynein and dynactin are localized to astral microtubules and at cortical sites in mitotic epithelial cells. Curr Biol 8, 541–544.

Cadart C, Zlotek-Zlotkiewicz E, Le Berre M, Piel M, Matthews HK (2014). Exploring the function of cell shape and size during mitosis. Dev Cell 29, 159–169.

den Elzen N, Buttery CV, Maddugoda MP, Ren G, Yap AS (2009). Cadherin adhesion receptors orient the mitotic spindle during symmetric cell division in mammalian epithelia. Mol Biol Cell 20, 3740–3750.

Desai A, Murray A, Mitchison TJ, Walczak CE (1999). The use of Xenopus egg extracts to study mitotic spindle assembly and function in vitro. Methods Cell Biol 61, 385–412.

Dinarina A, Pugieux C, Corral MM, Loose M, Spatz J, Karsenti E, Nedelec F (2009). Chromatin shapes the mitotic spindle. Cell 138, 502–513.

Dumont S, Mitchison TJ (2009a). Compression regulates mitotic spindle length by a mechanochemical switch at the poles. Curr Biol 19, 1086–1095.

Dumont S, Mitchison TJ (2009b). Force and length in the mitotic spindle. Curr Biol 19, R749–R761.

Emanuele MJ, Stukenberg PT (2007). Xenopus Cep57 is a novel kinetochore component involved in microtubule attachment. Cell 130, 893–905.

Fink J, Carpi N, Betz T, Betard A, Chebah M, Azioune A, Bornens M, Sykes C, Fetler L, Cuvelier D, Piel M (2011). External forces control mitotic spindle positioning. Nat Cell Biol 13, 771–778.

Goshima G, Scholey JM (2010). Control of mitotic spindle length. Annu Rev Cell Dev Biol 26, 21–57.

Grill SW, Hyman AA (2005). Spindle positioning by cortical pulling forces. Dev Cell 8, 461–465.

Hazel J, Krutkramelis K, Mooney P, Tomschik M, Gerow K, Oakey J, Gatlin JC (2013). Changes in cytoplasmic volume are sufficient to drive spindle scaling. Science 342, 853–856.

Jaffe AB, Kaji N, Durgan J, Hall A (2008). Cdc42 controls spindle orientation to position the apical surface during epithelial morphogenesis. J Cell Biol 183, 625–633.

Juschke C, Xie Y, Postiglione MP, Knoblich JA (2014). Analysis and modeling of mitotic spindle orientations in three dimensions. Proc Natl Acad Sci USA 111, 1014–1019.

Kotak S, Busso C, Gonczy P (2012). Cortical dynein is critical for proper spindle positioning in human cells. J Cell Biol 199, 97–110.

Kotak S, Gonczy P (2013). Mechanisms of spindle positioning: cortical force generators in the limelight. Curr Opin Cell Biol 25, 741–748.

Lancaster OM, Le Berre M, Dimitracopoulos A, Bonazzi D, Zlotek-Zlotkiewicz E, Picone R, Duke T, Piel M, Baum B (2013). Mitotic rounding alters cell geometry to ensure efficient bipolar spindle formation. Dev Cell 25, 270–283.

Lazaro-Dieguez F, Cohen D, Fernandez D, Hodgson L, van Ijzendoorn SC, Musch A (2013). Par1b links lumen polarity with LGN-NuMA positioning for distinct epithelial cell division phenotypes. J Cell Biol 203, 251–264.

Maiato H, DeLuca J, Salmon ED, Earnshaw WC (2004). The dynamic kinetochore-microtubule interface. J Cell Sci 117, 5461–5477.

McNally FJ (2013). Mechanisms of spindle positioning. J Cell Biol 200, 131–140.

Minc N, Burgess D, Chang F (2011). Influence of cell geometry on division-plane positioning. Cell 144, 414–426.

Mitsushima M, Aoki K, Ebisuya M, Matsumura S, Yamamoto T, Matsuda M, Toyoshima F, Nishida E (2010). Revolving movement of a dynamic cluster of actin filaments during mitosis. J Cell Biol 191, 453–462.

Mogilner A, Craig E (2010). Towards a quantitative understanding of mitotic spindle assembly and mechanics. J Cell Sci 123, 3435–3445.

Nakajima Y, Meyer EJ, Kroesen A, McKinney SA, Gibson MC (2013). Epithelial junctions maintain tissue architecture by directing planar spindle orientation. Nature 500, 359–362.

O'Connell CB, Wang YL (2000). Mammalian spindle orientation and position respond to changes in cell shape in a dynein-dependent fashion. Mol Biol Cell 11, 1765–1774.

Peyre E, Jaouen F, Saadaoui M, Haren L, Merdes A, Durbec P, Morin X (2011). A lateral belt of cortical LGN and NuMA guides mitotic spindle movements and planar division in neuroepithelial cells. J Cell Biol 193, 141–154.

Qin Y, Meisen WH, Hao Y, Macara IG (2010). Tuba, a Cdc42 GEF, is required for polarized spindle orientation during epithelial cyst formation. J Cell Biol 189, 661–669.

Reinsch S, Karsenti E (1994). Orientation of spindle axis and distribution of plasma membrane proteins during cell division in polarized MDCKII cells. J Cell Biol 126, 1509–1526.

Thery M, Bornens M (2006). Cell shape and cell division. Curr Opin Cell Biol 18, 648–657.

Thery M, Jimenez-Dalmaroni A, Racine V, Bornens M, Julicher F (2007). Experimental and theoretical study of mitotic spindle orientation. Nature 447, 493–496.

Thery M, Racine V, Pepin A, Piel M, Chen Y, Sibarita JB, Bornens M (2005). The extracellular matrix guides the orientation of the cell division axis. Nat Cell Biol 7, 947–953.

Toyoshima F, Matsumura S, Morimoto H, Mitsushima M, Nishida E (2007). PtdIns(3,4,5)P3 regulates spindle orientation in adherent cells. Dev Cell 13, 796–811.

Toyoshima F, Nishida E (2007). Integrin-mediated adhesion orients the spindle parallel to the substratum in an EB1- and myosin X-dependent manner. EMBO J 26, 1487–1498.

Walczak CE, Heald R (2008). Mechanisms of mitotic spindle assembly and function. Int Rev Cytol 265, 111–158.

Wang Y, Jin F, Higgins R, McKnight K (2014). The current view for the silencing of the spindle assembly checkpoint. Cell Cycle 13, 1694–1701.

Woodard GE, Huang NN, Cho H, Miki T, Tall GG, Kehrl JH (2010). Ric-8A and Gi alpha recruit LGN, NuMA, and dynein to the cell cortex to help orient the mitotic spindle. Mol Cell Biol 30, 3519–3530.

Wuhr M, Chen Y, Dumont S, Groen AC, Needleman DJ, Salic A, Mitchison TJ (2008). Evidence for an upper limit to mitotic spindle length. Curr Biol 18, 1256–1261.

Zheng Z, Zhu H, Wan Q, Liu J, Xiao Z, Siderovski DP, Du Q (2010). LGN regulates mitotic spindle orientation during epithelial morphogenesis. J Cell Biol 189, 275–288.